SUPPLEMENTAL METHODS

Tail Cuff Blood Pressure Measurement

Daily blood pressure measurements were performed with a mouse tail cuff plethysmograph (IITC Life Science Inc., Woodland Hills) by the same female operator (Y.L.) in a designated quiet room. Mice were habituated for ≥10 days prior to initiation of therapy by allowing their spontaneous entry into the restraint tube and subsequent adjustment of the tube length to limit motion. The cuff was placed at the base of the tail. System temperature was set at 34° C. Fifteen sequential blood pressure measurements were made, the first five of which were used for acclimation and the last ten of which were then averaged.

Echocardiography

High-frequency (40 MHz) transthoracic echocardiography (Vevo 2100, VisualSonics Inc., Toronto, Canada) was performed using a parasternal long-axis and sequential parasternal short-axis imaging planes to assess regional wall motion. LV dimensions at end-systole and end-diastole and fractional shortening (percent change in LV diameter normalized to end-diastole) were measured from the parasternal long-axis view using linear measurements of the LV at the level of the mitral leaflet tips during diastole. Radial strain was calculated using speckle-tracking echocardiography from a summation of mid- and apical short-axis images view and was quantified as the average of a standard single 6-segment model at the mid, and 4-segmental model at the apex. Stroke volume was calculated as the product of the left ventricular outflow tract cross-sectional area and time-velocity integral on pulsed-wave Doppler. The presence versus absence of any wall motion abnormalities was made by an experienced observer blinded to condition.

Spatial Assessment of Perfusion by Microspheres

In animals not undergoing CT coronary angiography, immediately after echocardiography, animals were intubated and placed on mechanical ventilation using weight-adjusted tidal volumes. A left lateral thoracotomy was performed to expose the left ventricular apex, through which a 23 g needle was placed to infuse 200 μl of a 1% w/v solution of fluorescently-labeled polystyrene microspheres 3-8 μm in diameter (Duke Scientific Corp., Palo Alto, California). Microspheres were allowed to circulate for 2 minutes. The heart was removed and cut into seven equal-thickness short-axis sections. Digital images of the basal aspect of all sections were acquired under ultraviolet light and the summed area devoid of fluorescent microspheres summed for all sections was measured and expressed as a ratio to total summed left ventricular area.

Flow Cytometry

Flow cytometry was used to assess platelet surface adhesion molecule expression. Whole blood from wild-type mice treated for 7 days with ponatinib or vehicle (n=3 each) was obtained in citrated tubes and centrifuged to obtain platelet-rich plasma. Primary rat anti-mouse monoclonal antibodies (5 μg) against either P-selectin (RB40.34, BD Biosciences) or GPIbα (R300, Emfret Analytics, Eibelstadt, Germany) were added to 200 mL aliquots. Platelets were than washed in phosphate-buffered saline containing 2% bovine serum albumin, and secondary staining was performed with FITC-labeled isotype-specific anti-rat secondary antibody (RG11 or RG7, BD Biosciences). Flow cytometry (FACSCanto II, BD Biosciences) was performed gated to the platelet window on forward and side scatter. Data are expressed as the average of the geometric mean for fluorescence intensity.

Statistical Analysis:

Data analysis was performed with Prism v7.0a (Graph Pad, La Jolla, California). Continuous variables that were normally distributed are displayed as mean ±SD unless stated

otherwise; whereas those that were not normally distributed are displayed as box-whisker plots with a bar representing median, box representing 25-75% confidence intervals, and whiskers representing range. Student *t* test (paired or unpaired) were performed for comparisons of normally distributed data. For non-normally distributed data, either a Mann-Whitney *U* test or Wilcoxon signed-rank test was used as appropriate according to experimental conditions (paired data within a group versus group-wise comparisons). For multiple comparisons, a one-way ANOVA was performed for normally distributed data with post-hoc testing with Holm-Sidak's multiple comparisons correction. A Kruskal-Wallis test followed by Dunn's multiple comparison test was performed for non-normally distributed data. Differences in proportions (wall motion data) were compared using Fisher's exact test. Differences were considered significant at $p<0.05$.

SUPPLEMENTAL FIGURES AND TABLES

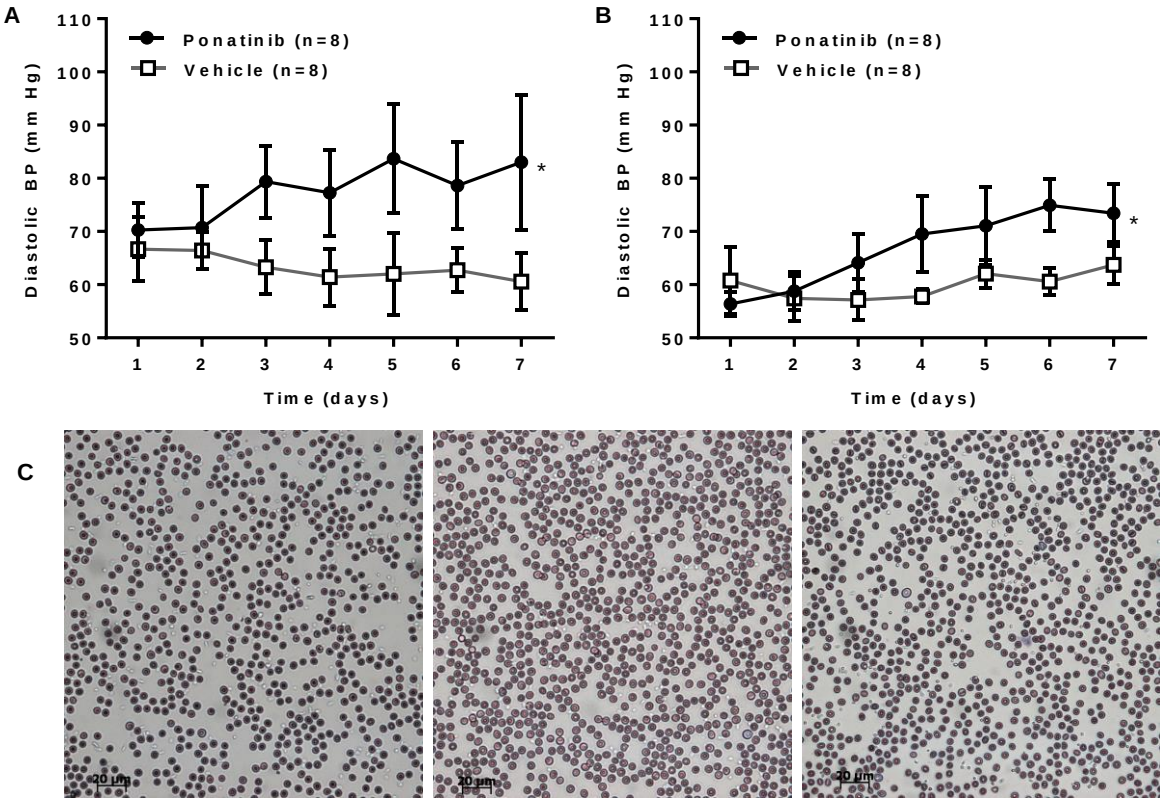

Supplemental Fig. 1. Tail cuff diastolic blood pressure (*BP*) measured from awake (**A**) wild-type C57Bl/6 mice and (**B**) ApoE-/- mice on Western-style diet (WSD) after initiation of ponatinib (30 mg/Kg/d) or vehicle. Animals were acclimatized to the procedure prior to initiation of therapy. *p<0.05 vs vehicle. (**C**) Wright-Giemsa stain of blood smears from 3 separate wild-type mice treated with ponatinib.

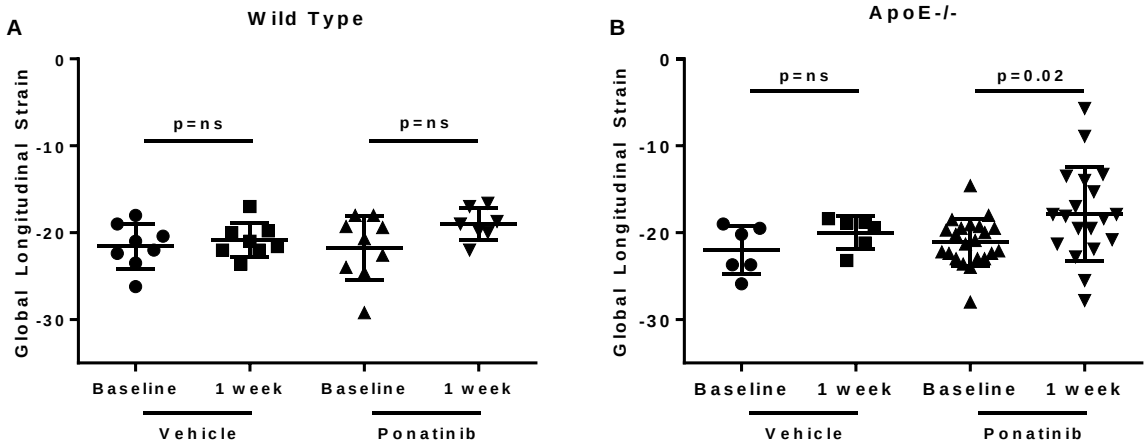

Supplemental Fig. 2. Mean (±SD) data for global longitudinal strain (dimensionless) from wild-type mice (**A**) and ApoE-/- mice on Western-style diet (**B**) treated with ponatinib (30 mg/kg/d) or vehicle (sham treatment).

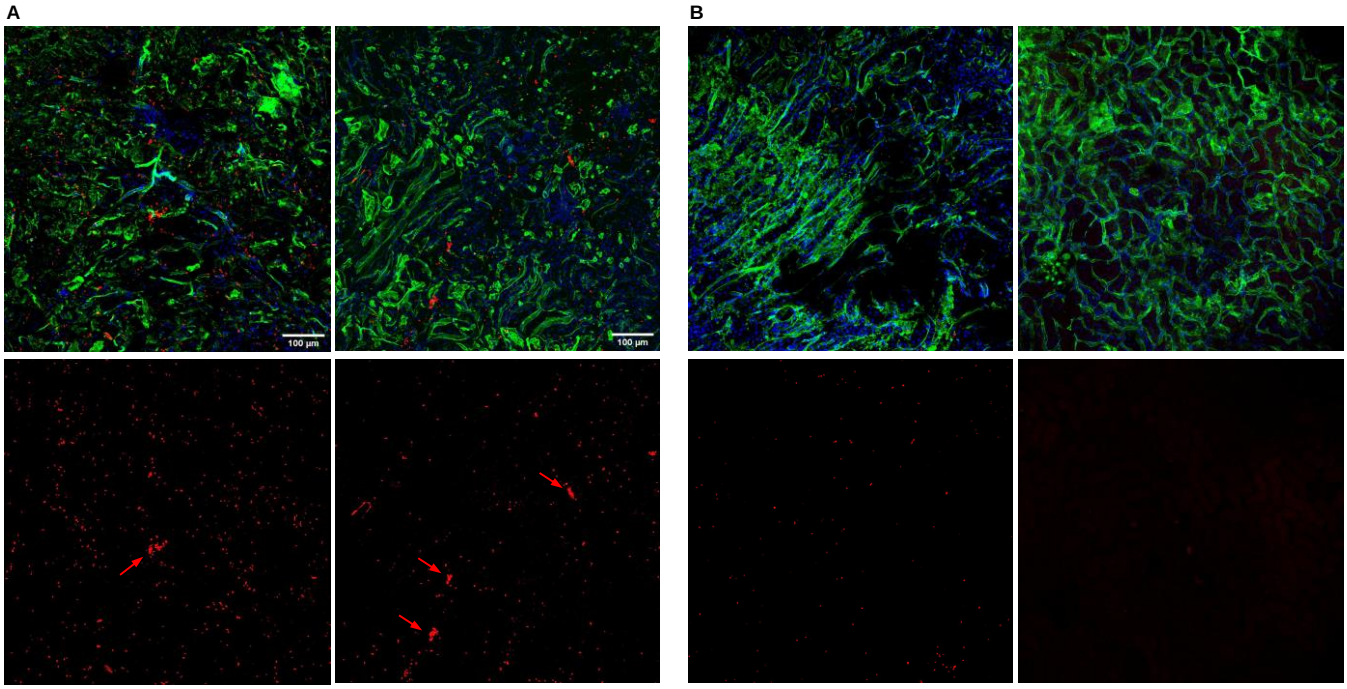

Supplemental Fig. 3 Fluorescent confocal microscopy of the renal cortex from (A) two separate ponatinib-treated wild-type mice, and (B) two separate vehicle-treated wild-type mice. Staining was performed with isolectin (green) for microvessels, Hoechst stain for nuclei (blue), and platelet CD41 immunohistochemistry (red). The bottom rows illustrate the red-channel alone to better display platelets. Platelet aggregates are highlighted by the red arrows.

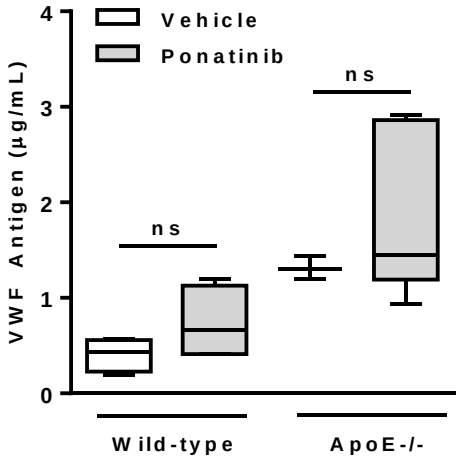

Supplemental Fig. 4. Box-whisker plots for plasma VWF antigen levels from ponatinib and vehicle-treated wild-type and ApoE-/- mice on Western-style diet.

Supplemental Table. Complete Blood Count (CBC) in Sham-treated and Ponatinib-treated Mice at 7 days*

	Sham (n=7)	Ponatinib (n=9)	p-value
White cell count (K/ml)	6.4±2.4	13.1±5.9	0.014
Hemoglobin (g/dL)	16.0±1.2	16.9±1.3	0.152
Hematocrit (%)	55.6±5.5	59.4±4.8	0.156
Platelets (K/mL)	678±362	573±254	0.503

*data combined for wild-type and ApoE-/- mice.

Video Legends

Video 1: Echocardiography in the parasternal long-axis plane demonstrating a large antero-apical wall motion abnormality in a ponatinb-treated ApoE-/- mouse.

Video 2: Echocardiography performed in the parasternal long-axis demonstrating a focal mid to basal inferior wall motion abnormalities.

Video 3: Echocardiography in the parasternal short-axis demonstrating an inferior and inferolateral wall motion abnormality.

Video 4: Intravital microscopy of the cremaster muscle of a sham-treated mouse injected with Rhodamine-6G illustrating normal leukocyte and platelet rapid rolling but no major adhesive events.

Video 5: Intravital microscopy of the cremaster muscle of a ponatinib-treated mouse injected with Rhodamine-6G illustrating the developing of labeled platelet strings (at the lesser curvature of the vessel).

Video 6: Intravital microscopy of the cremaster muscle of a ponatinib-treated mouse injected with Rhodamine-6G illustrating the dynamic development of a large labeled platelet network.

Video 7: Intravital microscopy of the cremaster muscle of a ponatinib-treated mouse injected with Rhodamine-6G illustrating the dynamic development of a stationary platelet leukocyte complex with eventual embolization.

Video 8: Intravital microscopy of the cremaster muscle of a ponatinib-treated mouse injected with Rhodamine-6G illustrating the dynamic development of a large platelet aggregate with eventual embolization.